AIAA SciTech
4-8 January 2016, San Diego, California, USA
54th AIAA Aerospace Sciences Meeting

AIAA 2016-1049

Instantaneous Pressure Reconstruction from Measured Pressure Gradient using Rotating Parallel Ray Method

Xiaofeng Liu[1], Jose Roberto Moreto[2] and Seth Siddle-Mitchell[3]
San Diego State University, San Diego, California, 92182-1308

This paper presents a novel pressure reconstruction method featuring rotating parallel ray omni-directional integration. It is an improvement over the circular virtual boundary integration method for non-intrusive instantaneous pressure measurement in incompressible flow field. Unlike the old method, where the integration path is originated from a virtual circular boundary at a finite distance from the integration domain, the new method utilizes parallel rays, which can be viewed as being originated from a distance of infinity, as guidance for integration paths. By rotating the parallel rays, omni-directional paths with equal weights coming from all directions toward the point of interest at any location within the computation domain are generated, thus eliminating the inherent location dependence of the integration weight in the old algorithm. By implementing this new algorithm, the accuracy of the reconstructed pressure for a synthetic rotational flow in terms of r.m.s. error from theoretical values is reduced from 1.03% to 0.30%. Improvement is further demonstrated from the comparison of the reconstructed pressure with the direct numerical simulation generated pressure from the Johns Hopkins University isotropic turbulence database (JHTDB).

Nomenclature

α	=	rotation angle of the rotating parallel rays
d	=	distance from a ray to the geometric center of the pressure reconstruction domain
C_p	=	pressure coefficient
$\delta\alpha$	=	increment of the rotation angle of the rotating parallel rays
δd	=	distance between adjacent parallel rays
δh	=	grid size of the computation domain
δt	=	time interval between adjacent PIV image exposures
m	=	$(m+1)$ is the total number of nodal points in the x-dimension
n	=	$(n+1)$ is the total number of nodal points in the y-dimension
p	=	pressure
r	=	radial distance from center of solid body rotation
i	=	index of nodal points in the x-direction
j	=	index of nodal points in the y-direction
ω	=	angular rotation rate of solid-body rotation

I. Introduction

PRESSURE distribution plays a crucial role in determining the flow phenomena and the system performance for a variety of applications involving fluid flow. For example, pressure is responsible for the lift and form drag acting on a moving body in fluid. Wall pressure fluctuations result in excitation of structures, leading to flow-induced vibrations and acoustic noise[1] (Blake 1986). In turbulence research, the pressure diffusion and the pressure-strain tensors are key unresolved parameters in modeling of turbulence[2, 3] (Pope 2000; Girimaji 2000). Pressure is also essential for understanding and modeling cavitation[4, 5] (Arndt 2002; Brennen 1995).

---

[1] Assistant Professor, Department of Aerospace Engineering, SDSU. AIAA Associate Fellow. Email: Xiaofeng.Liu@mail.sdsu.edu.
[2] Graduate Research Assistant, SDSU-UCSD Joint-Doctoral Program, College of Engineering, SDSU.
[3] Graduate Research Assistant, Department of Aerospace Engineering, SDSU. AIAA Student Member.

Because of the importance of the pressure information in flow field, efforts in developing non-intrusive pressure measurement techniques have been carried out in the past decade in the fluids community. Motivated by the lack of appropriate means for instantaneous spatial pressure distribution measurements, Liu and Katz[6-9] (2003, 2006, 2008, and 2013) have introduced and developed a novel non-intrusive technique capable of measuring the instantaneous spatial pressure, velocity and material acceleration distributions simultaneously over a sample area in a turbulent flow field. With the viscous term being negligible for high Reynolds number incompressible flow away from wall, the material acceleration is the dominant term that balances the pressure gradient. Once the material acceleration is obtained experimentally, the pressure gradient is known. Further integrating it will obtain the pressure. This is the roadmap introduced in Liu and Katz[6-7] (2003 and 2006). Initially, this technique utilized a four-exposure PIV (Particle Image Velocimetry) system, which consists of two 2K×2K CCD cameras and perpendicularly polarized Nd:Yag lasers, to measure the in-plane distribution of material acceleration by comparing the velocity of the same group of particles at different time, and then integrate it to obtain the pressure distribution. Starting in spring 2010, the four-exposure PIV system has been replaced by a time-resolved PIV system which consists of a high speed camera and a high repetition rate laser. A so-called *Circular Virtual Boundary, Omni-Directional Integration* over the entire measurement domain for pressure reconstruction was introduced by Liu and Katz[6-9]. The robustness of this integration method has been confirmed by Charonko *et al*[10] (2010), and utilized by several groups, e.g., Dabiri *et al*[11] (2014). Spatial integration of the measured acceleration field based on time-resolved PIV measurements to obtain the pressure distribution has also been used by van Oudheusden[12] (2008) and Ragni *et al*[13] (2009).

Besides the spatial integration method, de Kat and van Oudheusden[14-15] (2010, 2012) and Violato *et al*[16] (2011) use a *Poisson equation solver* to calculate the pressure from time resolved PIV measurements (see also van Oudheusden[17] 2013). More recently, an improved Poisson equation approach is proposed by Auteri *et al*[18] (2015). Following the advent of time-resolved PIV, the pressure reconstruction has also been adapted for measuring the temporal derivatives of surface pressure distribution, which is further used for estimating the acoustic pressure radiated from a surface[19-21] (Haigermoser 2009, Koschatzky *et al* 2010, and Moore *et al* 2010).

In addition to the omni-directional integration and the Poisson equation approaches, recently a so-called *least-square reconstruction* approach[22] (Jeon *et al*, 2015) is used for experimentally obtaining instantaneous pressure field in a wake of a separated flow over an airfoil. This approach is also referred to as *direct matrix inversion* by Liu and Katz[7] (2006).

One of the prominent difficulties in non-intrusive pressure measurement is how to reconstruct the pressure from the measured pressure gradient (or material acceleration as its dominant contributor) which is inevitably embedded with measurement errors. By minimizing the influence of errors in the measured data, the *Circular Virtual Boundary, Omni-Directional Integration* provides an effective method to reconstruct the pressure field. However, there is an inherent defect associated with the arrangement of the integration paths during the implementation of the algorithm, i.e., other than the points near the geometric center of the real integration domain, points at other places do not see a symmetric distribution of the virtual integration paths. This results in non-uniform weight of contribution to the final integration result at points away from the geometric center of the integration domain. As a result, the accuracy of the reconstructed pressure might be compromised, especially at places away from the geometric center of the computation domain.

In recognition of the inherent defect of the *circular virtual boundary algorithm*, this paper introduces a new algorithm featuring *rotating parallel ray* as integration path guidance. With the new algorithm, it is anticipated that the location dependence of the integration weight due to the defect in virtual path arrangement will be completely eliminated.

This paper will be arranged as follows: in section II, the old *circular virtual boundary algorithm* will be briefly reviewed. Subsequently in section III, the detailed explanation of the new *rotating parallel ray algorithm* for 2D pressure reconstruction will be presented. The capability and the accuracy of the new code in reconstructing the instantaneous pressure distribution using synthetic images of rotational stagnation flows will be shown in Section IV. Further testing and validation of the new code using the Johns Hopkins University isotropic turbulence database will be presented in Section V.

II. Review of the Circular Virtual Boundary Omni-Directional Integration Method

The essence of the pressure reconstruction method introduced by Liu and Katz[6-9] is the *Circular Virtual Boundary, Omni-Directional Integration* over the entire flow field. Detailed explanation of the method can be found in the literature mentioned above. However, for the sake of completeness of the current piece of work, which intrinsically stems from the framework formed by the old algorithm, essential description of the old method is briefed below.

The kernel of the old method is the *Omni-Directional Integration*. By summing up the errors embedded in the measured pressure gradients from all directions, the omni-integration minimizes the influence of the errors propagated to the final pressure result, so as to achieve a reliable and accurate pressure measurement. This pressure gradient integration arrangement is based on the fact that the pressure is a scalar potential, and therefore, spatial integration of the pressure gradient must be independent of the integration path. The discrete points distributed uniformly along the circular virtual boundary serve as guiding points to define the orientation and position of the integration paths. For example, as shown in Fig. 1(a), a group of "virtual" integration paths start at one point and end at other points on the virtual boundary, creating a ray pattern of integration guidelines that cover the real field of view. The use of virtual boundary is to alleviate the "clustering" of integration paths as described in Liu and Katz[7] (2006). The actual integration starts from and stops at the real boundaries, in a "zig-zag" fashion, along real nodal points that have the shortest distance to the integration guidelines. Each time the integration path crosses a certain internal node, the result of integration is stored in a data storage bin registered at that internal node. This procedure is repeated for all the virtual boundary nodes. Averaging all the values stored in the data bins provides the omni-directional integration, a procedure that minimizes the uncertainty caused by local errors in the measured pressure gradient (dominated by material acceleration for high Reynolds number flow away from wall). The pressure on the real boundary is initially obtained by simple line-integration along the real boundary, and is subsequently updated by the omni-integration results. Iteration using the updated boundary pressure leads to a converged boundary pressure distribution, as described in Liu and Katz[7-9] (2006, 2008 and 2013).

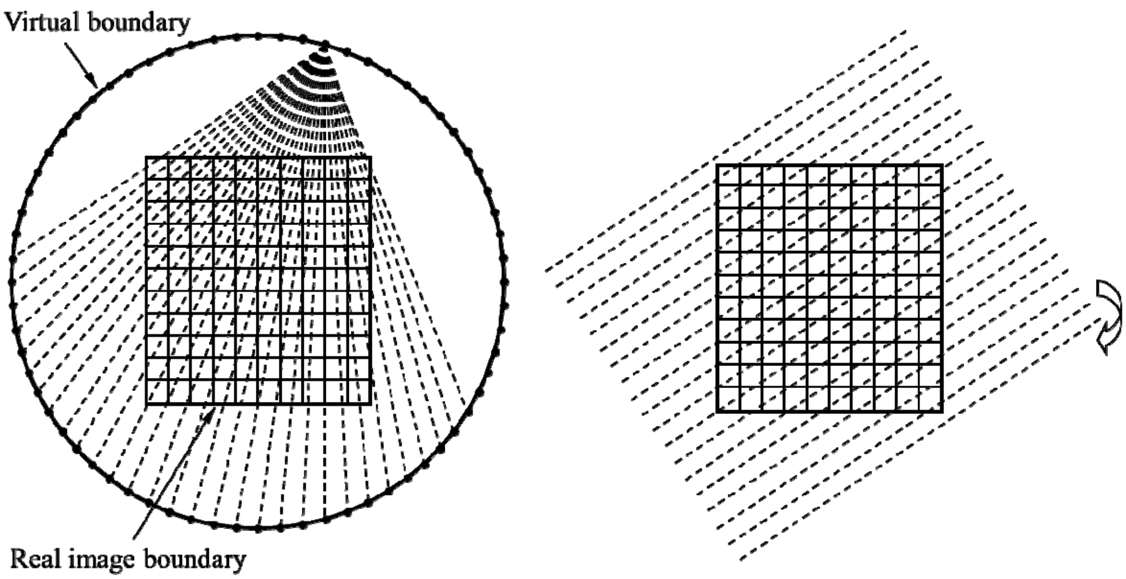

(a) The old circular virtual boundary omni-directional integration algorithm.

(b) The novel rotating parallel ray omni-directional integration algorithm.

Figure 1. The new and old omni-directional integration algorithms.

III. The Novel Rotating Parallel Ray Method

The novel *Rotating Parallel Ray Omni-Directional Integration* method is illustrated in Figure 1(b). Unlike the virtual boundary omni-directional method, where the virtual integration path is originated from a virtual circular boundary with a finite distance from the real boundary of the integration domain, the new method utilizes parallel rays as guidance for integration paths. The parallel rays can be effectively viewed as being originated from a distance of infinity from the real boundary. By rotating the parallel rays, effectively omni-directional paths with equal weights coming from all directions toward the point of interest at any location within the computation domain can be generated. In this way, the location dependence of the integration weight due to virtual path arrangement inherent in the old algorithm will be eliminated.

To implement the *Rotating Parallel Ray Omni-Directional Integration* method, the relative position of any arbitrary ray as a guideline with respect to the domain for pressure reconstruction is determined using the sketch shown in Figure 2, where *A*, *B*, *C* and *D* denote the four corner points of a rectangular computation domain with a total of $(m+1)\times(n+1)$ nodal points. Point $A(i=0, j=0)$ coincides with the origin of the *x-y* Cartesian coordinate system, while side *AB* goes along the *x*-axis and side *AD* along the *y*-axis. The two diagonals of the rectangular domain intercepts at point *E*. A line segment *EF*, with a segment length of *d*, forms an angle of α with respect to the horizontal reference line, i.e., the direction of the *x*-axis. A line *GH*, perpendicular to line *EF*, intercepts line *EF* at point *F*, side *AB* at *G* and side *BC* at *H*, respectively. For a definite variable combination of (α, d), the location and orientation of the guide line *GH*, along with coordinates of *G* and *H*, can be fully determined from simple trigonometric calculation. Thus the integration guideline and subsequently integration path is determined. By rotating the angle α and increasing the distance *d* in discrete fashion with constant increments, respectively, parallel ray integration guidelines can be formed, and the improved omni-directional integration can then be implemented.

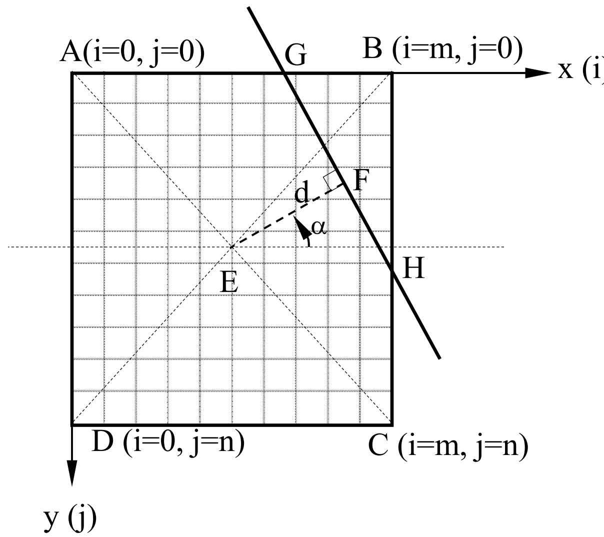

Figure 2. Interception points of an arbitrary line of the parallel ray on the boundaries of a pressure reconstruction domain.

IV. Accuracy Test using Synthetic Solid Body Rotational Flow

Based on the *Rotating Parallel Ray Omni-Directional Integration* algorithm described above, a 2D pressure reconstruction code is developed. To validate the code and to determine the accuracy of the new algorithm, we use synthetic images of solid-body rotation to reconstruct the pressure distribution and compare them with the theoretical values. Synthetic particle images, as shown in Fig. 3, serve as artificial PIV images, from which, velocity vector maps are obtained using a Johns Hopkins University in-house developed PIV analysis software (Roth and

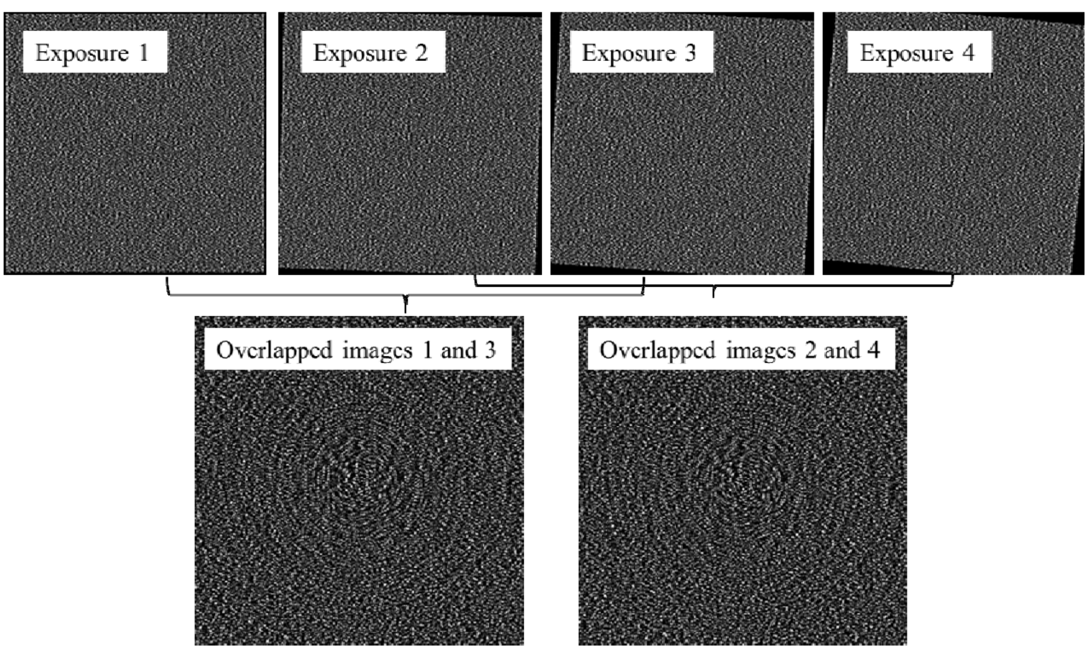

Figure 3. Synthetic images for solid-body rotational flow.

Katz[23], 2001). Following the procedures for the material acceleration calculation outlined in Liu and Katz[7] (2006), the material acceleration, which is exactly equivalent to the pressure gradient for inviscid flows, is then calculated. Finally the pressure reconstruction algorithm is applied and the pressure distribution is obtained.

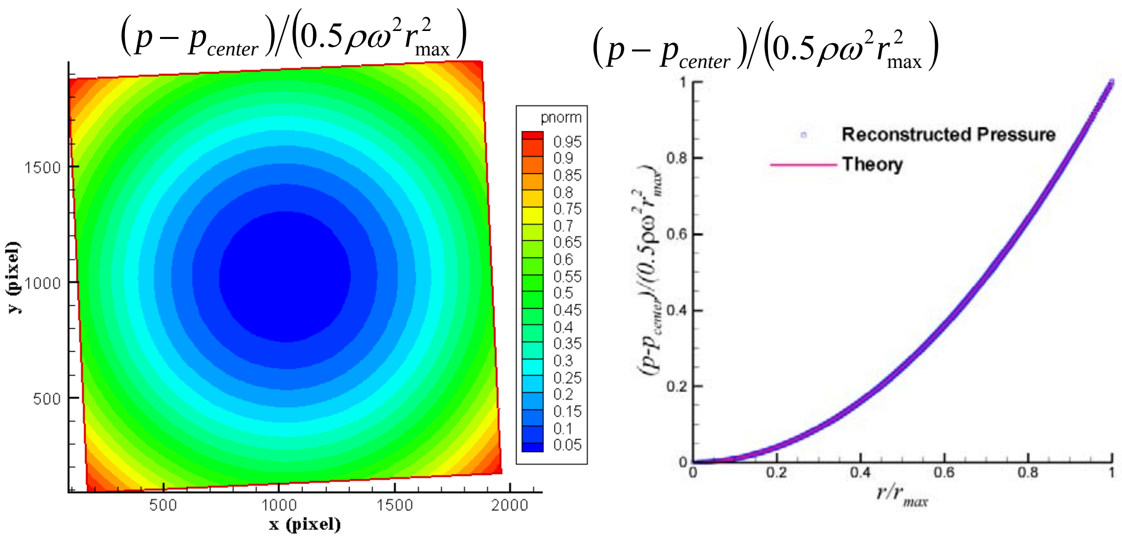

(a) (b)

Figure 4. (a) Spatial and (b) radial pressure distributions integrated from the material acceleration for the synthetic rotational flow using Rotating Parallel Ray Omni-Directional Integration method.

The parameters of the simulated flow are the same as those in Liu and Katz[7] (2006). The simulated seed particles are distributed homogeneously in a 2048×2048 pixels image using a random number generator available in Matlab. The particle concentration is set to maintain an average of 25 particles per interrogation window of 32×32 pixels. The particle size has a Gaussian distribution, with a mean diameter of 2.4 pixels and a standard deviation of 0.8 pixels. The intensity of the particle image is based on the local integration result of a Gaussian intensity distribution with a peak grayscale of 240 to reflect the CCD sensor integration effect. Particle overlapping is avoided by identifying occupied and unoccupied areas during the particle allocation process. Based on the first synthetic image, the subsequent three planes are generated by displacing the particles according to the local theoretical velocity, using the analytical expressions for the velocity fields. A bilinear interpolation is used for displacing the particles. The selected rotation rate of the synthetic solid-body-rotation is ω=0.0625/sec. The time interval between exposures is $\delta t = 0.5$ sec.

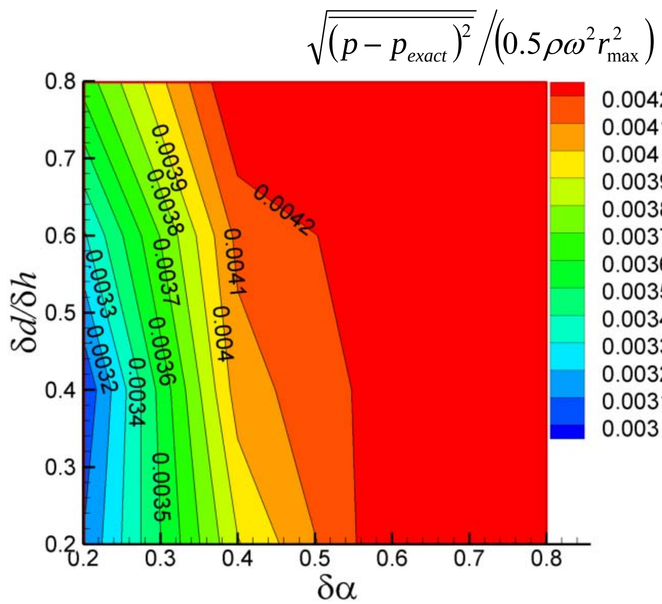

Figure 5. Contour plot of the standard deviation of the error in the reconstructed pressure obtained by using the rotating parallel ray algorithm for the synthetic solid-body rotation flow as a function of parallel ray spacing δd and ray rotating angle increment $\delta\alpha$.

Figure 4 shows the comparison of the radial distribution of the reconstructed pressure using the *Rotating Parallel Ray* Omni-Directional Integration method against the theoretical pressure values, which gives rise to a 0.30% of the standard deviation of the relative error, a significant improvement from the 1.03% relative error of the reconstructed pressure using the *Circular Virtual Boundary* Omni-Directional Integration method. During the computation, the rotating angle increment is $\delta\alpha = 0.3°$, and the parallel ray separation is $\delta d/\delta h = 0.4$.

Apparently, the standard deviation of the error of the reconstructed pressure using the *rotating parallel ray* algorithm is a function of the parallel ray spacing δd and the ray rotating angle increment $\delta\alpha$. Figure 5 shows the contour plot of the relative error of the reconstructed pressure using the rotating parallel ray algorithm for the synthetic solid-body rotation flow in the parameter space of ray spacing δd and ray rotating angle increment $\delta\alpha$. As shown in Fig. 5, the relative error of the reconstructed pressure varies from 0.3% to 0.4% within the range of $0.2 < \delta d/\delta h < 0.8$, and $0.2° < \delta\alpha < 0.8°$. Also within this parameter space, the relative error of the reconstructed pressure is less sensitive to the ray spacing δd than the ray rotating angle increment $\delta\alpha$, suggesting that $\delta\alpha$ is a more important parameter that affects the accuracy in the reconstructed pressure using the rotating parallel ray algorithm. Within the parameter domain investigated, there is no closed local minima of the relative error of the reconstructed pressure due to the limited size of the parameter space. However, the overal trend shows that the error of the reconstructed pressure decreases as $\delta\alpha$ decreses, suggesting a fine ray rotaional angle increment can bring in benefit for the improvement of the reconstructed pressure accuracy. Obviously a finer angle increment means a higher computational cost. The computational cost associated with parameter optimization will be investigated in the subsequent work of the project.

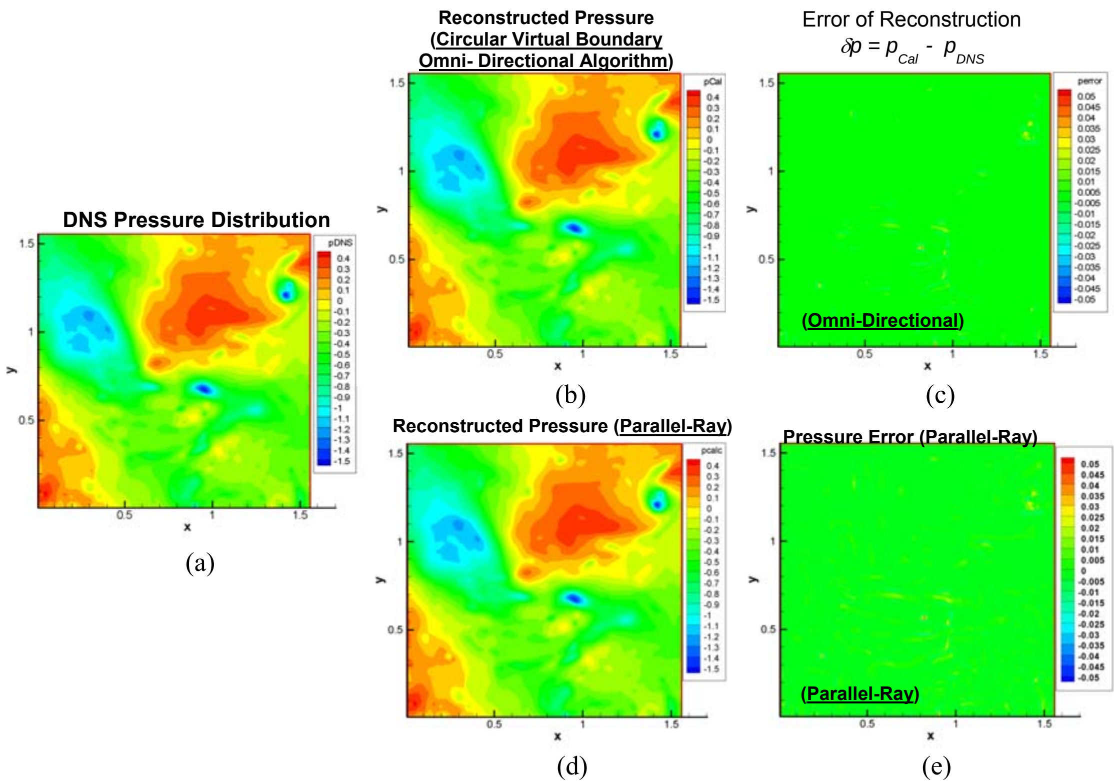

Figure 6. (a) DNS pressure distribution. (b) Reconstructed pressure using *Circular Virtual Boundary Omni-Directional Integration* algorithm. (c) Difference between the pressure reconstructed using the *Circular Virtual Boundary* algorithm and the DNS pressure. (d) Reconstructed pressure using *Rotating Parallel Ray Omni-Directional Integration* algorithm. (e) Difference between the pressure reconstructed using the *Rotating Parallel Ray* algorithm and the DNS pressure.

V. Validation using the Johns Hopkins University isotropic turbulence database

To further validate the pressure reconstruction technique, we apply both the new and old pressure reconstruction codes to the pressure gradient fields of a forced isotropic turbulence in a direct numerical simulation (DNS) database. We then compare the “measured” pressure with the DNS pressure distribution.

The DNS data is obtained from the Johns Hopkins University turbulence database (JHTDB, see Li *et al*[24], 2008). It consists of results of a direct numerical simulation of forced isotropic turbulence on a 1024^3 periodic grid, using a pseudo-spectral parallel code. Energy is injected at each step of simulation to maintain steady state conditions. This injection keeps the energy in modes with wave-numbers less or equal to 2 constant. The database provides 1,024 instantaneous realizations, which includes the 3 components of the velocity and the pressure in a $2\pi\times2\pi\times2\pi$ domain. The simulation time-step is 0.0002, and the time interval between stored samples in the database is 0.002, both of which are smaller than the Kolmogorov time scale of 0.0446. The grid size is 0.00614, which is slightly larger than the Kolmogorov length scale of 0.00287. The Taylor-scale Reynolds number for the isotropic flow is 433.

As a preliminary effort of the investigation, a sample plane with 256×256 grid nodal points is selected from the JHTDB isotropic turbulence database, as shown in Fig. 6(a). The pressure distributions reconstructed from the DNS pressure gradient using the *Circular Virtual Boundary Omni-Directional Integration* algorithm and the *Rotating Parallel Ray Omni-Directional Integration* algorithm, are presented in Fig. 6(b) and (d), respectively, with the corresponding error distributions shown in Fig. 6(c) and (e). As can be seen from these figures, both methods faithfully reproduced the isotropic turbulence pressure distribution, without noticeable differences between themselves and the DNS pressure distributions. However, further investigation of the statistics in terms of the standard deviation of the reconstructed pressure error normalized by the standard deviation of the isotropic turbulence pressure fluctuation indicates that the $\sigma_{\delta p}/\sigma_{p\mathrm{DNS}}$ = 0.57% for the circular virtual boundary algorithm and 0.56% for the rotating parallel-ray algorithm, indicating the performance of the latter is slightly better than the former, thus in agreement with the trend observed from the synthetic solid-body rotational flow.

VI. Conclusion and future work

A novel pressure reconstruction method featuring *Rotating Parallel Ray Omni-Directional Integration* is introduced. Equal weights of integration involvement can be achieved, thus eliminating the location dependence of the integration weight inherent in the old *Circular Virtual Boundary Omni-Directional Integration* algorithm. The accuracy of the new algorithm tested with a synthetic rotational flow shows that the normalized r.m.s. error is reduced from 1.03% to 0.30%. Improvement is further demonstrated from tests using the Johns Hopkins University isotropic turbulence database (JHTDB).

The standard deviation of the error of the reconstructed pressure using the *rotating parallel ray* algorithm is a weak function of the parallel ray spacing δd yet a relatively strong function of the ray rotating angle increment $\delta\alpha$, suggesting that $\delta\alpha$ is a more important parameter that affects the accuracy in the reconstructed pressure using the rotating parallel ray algorithm. The relative error of the reconstructed pressure varies from 0.3% to 0.4% within the range of $0.2 < \delta d/\delta h < 0.8$, and $0.2° < \delta\alpha < 0.8°$. Within the parameter range investigated, the error of the reconstructed pressure decreases as $\delta\alpha$ decreses, suggesting a fine ray rotaional angle increment can bring in benefit for the improvement of the reconstructed pressure accuracy.

Along with continuing validation and refinement, the pressure reconstruction code based on the new *rotating parallel ray omni-directional integration* method will be applied to projects to be conducted at the new San Diego State University water tunnel facility.

Acknowledgments

The financial support from the UGP program of the San Diego State University for this research project is gratefully acknowledged.

References

[1]Blake, W.K., *Mechanics of Flow-Induced Sound and Vibration*, Academic, New York, 1986.

[2]Pope, S.B., *Turbulent Flows*, Cambridge University Press, Cambridge, 2000.

Periodicals

[3]Girimaji, S.S., "Pressure-Strain Correlation Modeling of Complex Turbulent Flows", *J. Fluid Mech.*, Vol. 422, November 2000, pp.91-123.

[4]Arndt, R. E. A., "Cavitation in vortical flows," *Annu. Rev. Fluid Mech.* 34, 143, January 2002.

[5]Brennen, C. E., *Cavitation and bubble dynamics*, Oxford University Press, Oxford, 1995.

[6]Liu, X. and Katz, J., "Measurements of Pressure Distribution by Integrating the Material Acceleration", Cav03-GS-14-001, *Proc. of the 5th International Symposium on Cavitation (Cav2003)*, Osaka, Japan, Nov. 1-4, 2003.

[7]Liu, X. and Katz, J., "Instantaneous Pressure and Material Acceleration Measurements using a Four Exposure PIV System," *Exp. Fluids*, Vol. 41, No. 2, August 2006, pp227-240.

[8]Liu, X. and Katz, J., "Cavitation Phenomena Occurring due to Interaction of Shear Layer Vortices with the Trailing Corner of a 2D Open Cavity," *Physics of Fluids*, Vol. 20, No. 4, April 2008, 041702, DOI:10.1063/1.2897320.

[9]Liu, X. and Katz, J., "Vortex-Corner Interactions in a Cavity Shear Layer Elucidated by Time Resolved Measurements of the Pressure Field," *J. Fluid Mech.*, Vol. 728, August 2013, pp 417-457. DOI: 10.1017/jfm.2013.275.

[10]Charonko, J. J., King, C. V., Smith, B. L. and Vlachos, P. P., "Assessment of Pressure Field Calculations from Particle Image Velocimetry Measurements," *Meas. Sci. Technol.*, Vol. 21, No.10, October 2010, 105401.

[11]Dabiri, J.O., Bose, S., Gemmell, B.J., Colin, S.P., and Costello, J.H., "An algorithm to estimate unsteady and quasi-steady pressure fields from velocity field measurements", *J. of Experimental Biology*, 2014 : doi: 10.1242/jeb.092767

[12]Van Oudheusden, B. W. "Principles and Application of Velocimetry-Based Planar Pressure Imaging in Compressible Flows with Shocks," *Exp. Fluids*, Vol. 45, No. 4, October 2008, pp. 657–674.

[13]Ragni, D., Ashok, A., Van Oudheusden, B. W. and Scarano, F., "Surface Pressure and Determination of a Transonic Aerofoil Based on Particle Image Velocimetry," *Meas. Sci. Technol.*, Vol. 20, No. 7, July 2009, 074005.

[14]De Kat, R. and Van Oudheusden, B. W., "Instantaneous planar pressure from PIV: analytic and experimental test-cases". In *15th International Symposium on Applications of Laser Techniques to Fluid Mechanics*, Lisbon, Portugal, July 5-8, 2010.

[15]De Kat, R. and Van Oudheusden, B. W. "Instantaneous planar pressure determination from PIV in turbulent flow", *Exp Fluids* Vol. 52, No. 5, pp. 1089–1106, May 2012.

[16]Violato, D., Moore, P. and Scarano, F., "Lagrangian and Eulerian Pressure Field Evaluation of Rod-Airfoil Flow from Time-Resolved Tomographic PIV", *Exp. Fluids*., Vol.50, No. 4, April 2011, pp. 1057–1070.

[17]Van Oudheusden, B. W., "PIV-based pressure measurement," *Meas. Sci. Technol.* Vol. 24, No.3, March 2013, 032001.

[18]Auteri, F., Carina, M., Zag glia, D., Montagnon, D., Libertine, G., Mars, C. B. and Zanetti, A., "A Novel Approach for Reconstructing Pressure from PIV Velocity Measurements," *Exp Fluids*, Vol, 56 , No.45, February 2015, DOI 10.1007/s00348-015-1912-z.

[19]Haigermoser, C. "Application of an acoustic analogy to PIV data from rectangular cavity flows," *Exp. Fluids*, Vol. 47 No. 1, July 2009, pp. 145–157.

[20]Koschatzky, V., Moore, P. D., Westerweel, J., Scarano, F. and Boersma, B. J., "High Speed PIV Applied to Aerodynamic Noise Investigation," *Exp. Fluids* Vol. 50, No.4, April 2011, pp. 863–876.

[21]Moore, P., Lorenzoni, V. and Scarano, F., "Two techniques for PIV-based aeroacoustic prediction and their application to a rod-aerofoil experiment," *Exp. Fluids* Vol. 50, No.4, April 2011, pp. 877-885.

[22]Jeon, Y.J., Chatellier, L., Beaudoin, A., and David, L., "Least-square reconstruction of instantaneous pressure field around a body based on a directly acquired material acceleration in time-resolved PIV", *11th International Symposium on Particle Image Velocimetry – PIV15*, Santa Barbara, California, September 14-16, 2015.

[23]Roth, G. I. and Katz, J., "Five techniques for increasing the speed and accuracy of PIV interrogation", *Meas. Sci. Technol*. Vol. 12, No. 3, March 2001, pp. 238–245.

[24]Li Y, Perlman E, Wan M, Yang Y, Meneveau C, Burns R, Chen S, Szalay A and Eyink G, "A public turbulence database cluster and applications to study Lagrangian evolution of velocity increments in turbulence", *J of Turbulence*. Vol. 9, No. 31, January 2008, pp. 1-29.